Modulation of Tropical Cyclogenesis by Convectively Coupled Kelvin Waves

ROSIMAR RIOS-BERRIOS,[a] BRIAN H. TANG,[b] CHRISTOPHER A. DAVIS,[a] AND JONATHAN MARTINEZ[c]

[a] *National Science Foundation National Center for Atmospheric Research, Boulder, Colorado*
[b] *University at Albany, State University of New York, Albany, New York*
[c] *Cooperative Institute for Research in the Atmosphere, Fort Collins, Colorado*

(Manuscript received 22 March 2024, in final form 22 June 2024, accepted 18 July 2024)

ABSTRACT: Tropical cyclone numbers can vary from week to week within a hurricane season. Recent studies suggest that convectively coupled Kelvin waves can be partly responsible for such variability. However, the precise physical mechanisms responsible for that modulation remain uncertain partly due to the inability of previous studies to isolate the effects of Kelvin waves from other factors. This study uses an idealized modeling framework—called an aquaplanet—to uniquely isolate the effects of Kelvin waves on tropical cyclogenesis. The framework also captures the convective-scale dynamics of both tropical cyclones and Kelvin waves. Our results confirm an uptick in tropical cyclogenesis after the passage of a Kelvin wave—twice as many tropical cyclones form 2 days after a Kelvin wave peak than at any other time lag from the peak. A detailed composite analysis shows anomalously weak ventilation during and after (or to the west of) the Kelvin wave peak. The weak ventilation stems primarily from anomalously moist conditions, with weaker vertical wind shear playing a secondary role. In contrast to previous studies, our results demonstrate that Kelvin waves modulate both kinematic and thermodynamic synoptic-scale conditions that are necessary for tropical cyclone formation. These results suggest that numerical models must capture the three-dimensional structure of Kelvin waves to produce accurate subseasonal predictions of tropical cyclone activity.

SIGNIFICANCE STATEMENT: Anticipating active tropical cyclone periods several weeks in advance could help mitigate the loss of lives and property due to these phenomena. Recent studies suggest that a type of tropical cloud cluster—known as convectively coupled Kelvin waves—can promote tropical cyclone formation. Kelvin waves travel around the world and can be detected days to weeks in advance. We use a simplified numerical model to isolate the effects of Kelvin waves on tropical cyclone formation. Our unique approach confirms that tropical cyclones are more likely to form 2 days after a Kelvin wave than before the wave. We also demonstrate that—contrary to previous perception—the enhancement of tropical cyclogenesis is due to both more moisture and weaker wind currents following the waves.

KEYWORDS: Kelvin waves; Tropical cyclones; Moisture/moisture budget; Tropical variability

1. Introduction

More than four decades ago, scientists started to notice that tropical cyclones form in clusters followed by several weeks of little to no tropical cyclone activity (Gray 1979). Nowadays, this variability is known as subseasonal variability of tropical cyclogenesis—that is, a variable rate of tropical cyclone formation within a season. Accurately predicting such variability has strong societal implications because we would know 2–4 weeks in advance when to expect an active tropical cyclone period. Recent studies have discovered potential drivers of subseasonal tropical cyclone variability, including equatorial waves (Frank and Roundy 2006; Bessafi and Wheeler 2006; Ventrice et al. 2012a,b; Schreck et al. 2012; Ventrice and Thorncroft 2013; Schreck 2015; Feng et al. 2023; Lawton and Majumdar 2023), the Madden–Julian oscillation (MJO) (Frank and Roundy 2006; Maloney and Hartmann 2000a,b; Bessafi and Wheeler 2006; Klotzbach 2010; Klotzbach and Oliver 2014, 2015), and midlatitude Rossby waves (Zhang et al. 2016; Papin et al. 2020). This study focuses on a group of equatorial waves—known as convectively coupled Kelvin waves—and their potential modulation of tropical cyclogenesis.

Convectively coupled Kelvin waves (Kelvin waves hereafter) are important sources of tropical rainfall variability (Wheeler and Kiladis 1999; Roundy and Frank 2004; Straub and Kiladis 2003; Kiladis et al. 2009). These waves propagate eastward along the intertropical convergence zone (ITCZ), where they enhance or suppress rainfall over zonal wavelengths between 3000 and 7000 km and time periods between several days and several weeks. Their rainfall anomalies are coupled to wind, temperature, and water vapor perturbations (Wheeler and Kiladis 1999; Straub and Kiladis 2003; Yang et al. 2007; Roundy 2008; Kiladis et al. 2009; Nakamura and Takayabu 2022). Anomalous lower-tropospheric westerlies and upper-tropospheric easterlies appear to the west of (or behind) the Kelvin wave convection, while anomalous lower-tropospheric easterlies and upper-tropospheric westerlies appear to the east (Straub and Kiladis 2003; Roundy 2008; Kiladis et al. 2009; Nakamura and Takayabu 2022). Cool and moist anomalies are also observed in association with Kelvin

Supplemental information related to this paper is available at the Journals Online website: https://doi.org/10.1175/MWR-D-24-0052.s1.

Corresponding author: Rosimar Rios-Berrios, rberrios@ucar.edu

DOI: 10.1175/MWR-D-24-0052.1

waves, and those anomalies exhibit a westward tilt with height from the lower to the middle troposphere (Straub and Kiladis 2003; Roundy 2008; Kiladis et al. 2009; Nakamura and Takayabu 2022). Regional circulations in the tropics can be affected by the Kelvin wave anomalies on subseasonal time scales, which might, in turn, affect the environments where tropical cyclones form.

Early studies hypothesized that Kelvin waves played little role in tropical cyclogenesis, but recent studies have found a potential modulation of tropical cyclone formation by Kelvin waves (Frank and Roundy 2006; Bessafi and Wheeler 2006; Schreck et al. 2011, 2012; Ventrice et al. 2012a,b; Ventrice and Thorncroft 2013; Schreck 2015; Lawton and Majumdar 2023). A study that examined the convectively *active* structure of different types of equatorial waves at the time and location of tropical cyclogenesis did not find a signal associated with Kelvin waves (Frank and Roundy 2006). Subsequent studies, however, found above-average tropical cyclogenesis events during the convectively *suppressed* phase of Kelvin waves (Schreck et al. 2011, 2012; Ventrice et al. 2012a,b; Ventrice and Thorncroft 2013; Schreck 2015). This finding may be counterintuitive because rainfall amounts are relatively small during the suppressed phase, but midtropospheric humidification and convective organization are key processes preceding tropical cyclogenesis (Gray 1968; Bister and Emanuel 1997; Raymond et al. 1998; Nolan 2007; Rappin et al. 2010; Komaromi 2013; Zawislak and Zipser 2014; Helms and Hart 2015).

Several explanations exist in the literature for the enhancement of tropical cyclogenesis by Kelvin waves—focusing largely on the modulation of synoptic-scale conditions necessary for tropical cyclogenesis. For example, anomalous lower-tropospheric westerlies associated with the convectively suppressed phase of Kelvin waves may reduce the vertical wind shear magnitude and enhance the lower-tropospheric vorticity (Ventrice et al. 2012b; Schreck 2015). Intriguingly, a global study on the relationship between Kelvin waves and tropical cyclogenesis found little to no modulation of thermodynamic factors by the Kelvin waves (Schreck 2015). This finding led to the suggestion that "the dynamical effects from the Kelvin wave likely outweigh its thermodynamic impacts." A more recent study challenged this assumption by showing that Kelvin waves interacting with African easterly waves were associated with significant water vapor anomalies (Lawton et al. 2022). A follow-up study further found that Kelvin waves aided the development of African easterly waves into tropical cyclones via midtropospheric humidification and cloud-radiative interactions (Lawton and Majumdar 2023).

Despite the growing evidence that Kelvin waves modulate tropical cyclogenesis, several limitations prevent a generalization of the existing literature. First, previous studies were unable to isolate the influence of Kelvin waves from other factors. Some studies noted that most of the Kelvin waves identified in proximity to tropical cyclones coincided with an active MJO (Schreck 2015; Ventrice et al. 2012b). It is, therefore, difficult to attribute the anomalously favorable environmental conditions preceding tropical cyclogenesis solely to Kelvin waves. Second, previous studies used coarse-resolution datasets (such as reanalyses) that cannot capture the convective-scale dynamics of Kelvin waves *and* tropical disturbances/cyclones. Reanalyses also have a nonseparable contribution from the physics of the numerical model used in the data assimilation, and this will impart properties of parameterized convection into the analysis in an unquantified way. Third, previous studies typically characterized rainfall and convection using satellite-derived or satellite-estimated products, while examining other fields with reanalysis datasets and defining tropical cyclogenesis with best track data. There is no guarantee that these datasets are physically consistent with each other. Studies have shown that the location and intensity of tropical cyclones (especially tropical depressions and storms) can be inconsistent between reanalyses and best tracks (Schenkel and Hart 2012; Murakami 2014; Hodges et al. 2017).

Furthermore, previous studies have not examined the compound interactions between factors. For example, growing evidence suggests that the combination of vertical wind shear, moisture, and the underlying ocean temperatures is more critical for tropical cyclogenesis and intensification than vertical wind shear alone (Nolan and Rappin 2008; Davis and Ahijevych 2012; Ge et al. 2013; Tao and Zhang 2014; Rios-Berrios and Torn 2017; Alland et al. 2021a,b). To this end, Tang and Emanuel (2010) presented a theoretical framework considering the compound effects of vertical wind shear and thermodynamic factors, leading to the derivation of a ventilation index (Tang and Emanuel 2012, and described mathematically in section 2). This index is a proxy for the likelihood of dry, cool air being imported into a tropical disturbance by the vertically sheared environmental flow, which would be detrimental for tropical cyclogenesis. Hence, the index is skillful at distinguishing between developing and nondeveloping disturbances (Tang and Emanuel 2012), and it is also useful at diagnosing changes in tropical cyclone activity under different climates (Tang and Camargo 2014; Vecchi et al. 2019). It remains to be investigated if the combined anomalous winds and thermodynamics associated with Kelvin waves can modulate the ventilation index, which, in turn, may explain how Kelvin waves modulate tropical cyclogenesis.

In light of these limitations, we present herein an idealized modeling study that focuses on the relationship between Kelvin waves and tropical cyclogenesis. The objectives of this study are as follows:

- to investigate if a relationship between Kelvin waves and tropical cyclogenesis exists in an idealized modeling experiment,
- to determine if Kelvin waves modulate the dynamic *and* thermodynamic conditions necessary for tropical cyclogenesis, and
- to identify key physical processes that may explain how Kelvin waves influence tropical cyclogenesis.

To achieve these objectives, we use an aquaplanet configuration with the Model for Prediction Across Scales–Atmosphere (MPAS-A) (Skamarock et al. 2012). The aquaplanet configuration has no seasons, no land, and no El Niño or La Niña. A variable-resolution configuration yields convection-permitting resolution in the tropics to capture the convective-scale dynamics

associated with both Kelvin waves and tropical disturbances/cyclones (Rios-Berrios et al. 2023a, RDM23 hereafter). While the framework is a highly idealized representation of Earth, the simulation provides a complete and physically consistent dataset. Importantly, MPAS-A aquaplanet experiments capture Kelvin waves and other smaller-scale waves (e.g., easterly waves) but no MJO (Rios-Berrios et al. 2022, 2023a,b). The relative simplicity of this simulation, compared with the real atmosphere, allows a direct assessment of the mechanism of Kelvin wave influence on tropical cyclogenesis.

A major benefit of using the aquaplanet framework is its ability to simulate weather patterns similar to those observed on Earth's oceans (Fig. 1 and animation in the online supplemental material). Clouds and rainfall concentrate in a relatively narrow band along the intertropical convergence zone. Tropical cyclones form in the deep tropics and travel into the midlatitudes. The simulation used herein was described in detail by RDM23, who also demonstrated that the simulation captures realistic Kelvin waves, easterly waves, and tropical cyclones. The simulation setup, Kelvin wave identification, and other details of the methodology are briefly presented in section 2. The simulation confirms that Kelvin waves modulate tropical cyclogenesis via reduced ventilation, as discussed in sections 3 and 4. An analysis focusing solely on Kelvin waves, presented in section 5, confirms their modulation of both kinematic and thermodynamic synoptic-scale conditions necessary for tropical cyclogenesis. These results are summarized in section 6.

2. Methods

a. Experimental setup

We studied the relationship between convectively coupled Kelvin waves and tropical cyclogenesis using the aquaplanet simulation described by RDM23. The simulation used the MPAS-A model configured as a water-covered sphere with the dimensions of Earth. A temporally fixed, zonally symmetric SST profile provided the surface boundary condition. The SST had a maximum of 28.5°C at 10°N and decayed with latitude until reaching 0°C at 80°N and 60°S based on the formulation of Ballinger et al. (2015) (see Fig. 1 of RDM23). We included the diurnal cycle, but no seasons as given by fixed solar constant and declination angle with maximum insolation at the equator. These conditions yield a time-mean, zonal-mean state that closely resembles the climatological September conditions over the tropical Pacific (RDM23).

We used the Cheyenne supercomputing system (Computational and Information Systems Laboratory 2023) to produce a variable mesh having approximately 3-km cell spacing between 10°S and 30°N. The cell spacing gradually transitioned to 12.3-km cell spacing poleward of 30°S and 55°N (see Fig. 1 of RDM23). This configuration specified convection-permitting resolution within the region of warmest SSTs. The vertical grid had 75 levels stretching from 60-m vertical spacing near the surface to 500-m spacing between 10 km and the model top at 40 km. We used physics packages that are thoroughly tested for tropical cyclone studies, including the WSM6 microphysics

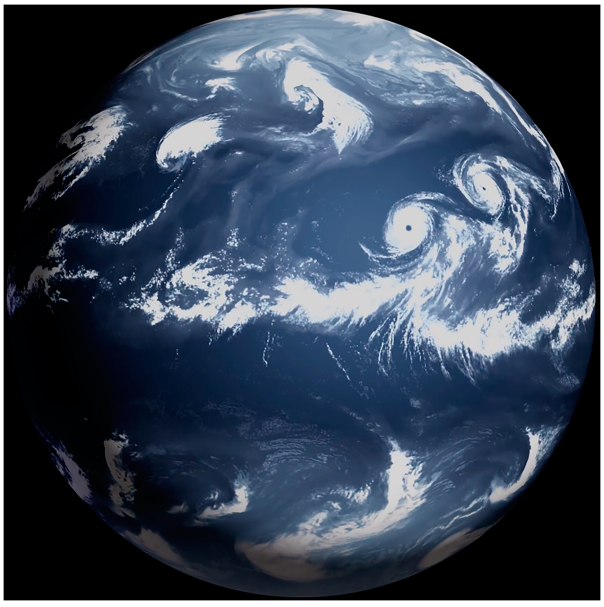

FIG. 1. Snapshot of outgoing longwave radiation from the MPAS-A aquaplanet simulation used in this study. An animated version is available in the supplemental material.

(Hong et al. 2006), the YSU planetary boundary layer scheme (Hong et al. 2004), RRTMG shortwave and longwave radiation (Mlawer et al. 1997; Iacono et al. 2008), and a scale-aware version of the new Tiedtke scheme (Wang 2022). Aerosols were radiatively inactive, and the ozone was given by a hemispheric symmetric distribution provided by the Aqua-Planet Experiment (Blackburn et al. 2013). The first month was considered model spinup; therefore, we only used the last 4 months in our analysis. The interested reader is referred to RDM23 for more details of the simulation setup.

b. Identification of Kelvin waves

We identified Kelvin waves using spatiotemporal filtering of rainfall rates interpolated on a 0.1° × 0.1° latitude–longitude grid. Rainfall rates were first averaged between 5°S and 10°N and then filtered following the steps (Wheeler and Weickmann 2001). These steps included the following:

1) detrending the data,
2) zero-padding the detrended data at the beginning of the time period,
3) applying a two-dimensional fast Fourier transform in space and time,
4) retaining eastward wavenumbers 1–14 and periods of 2.5–20 days, and
5) applying an inverse fast Fourier transform to obtain the filtered rainfall rates in time and longitude.

This method is effective at identifying Kelvin waves in MPAS-A aquaplanet simulations (Rios-Berrios et al. 2020, 2022, 2023b).

A recent study recommends using at least two different wave identification methods to confirm the presence of equatorial waves (Knippertz et al. 2022). Based on this recommendation,

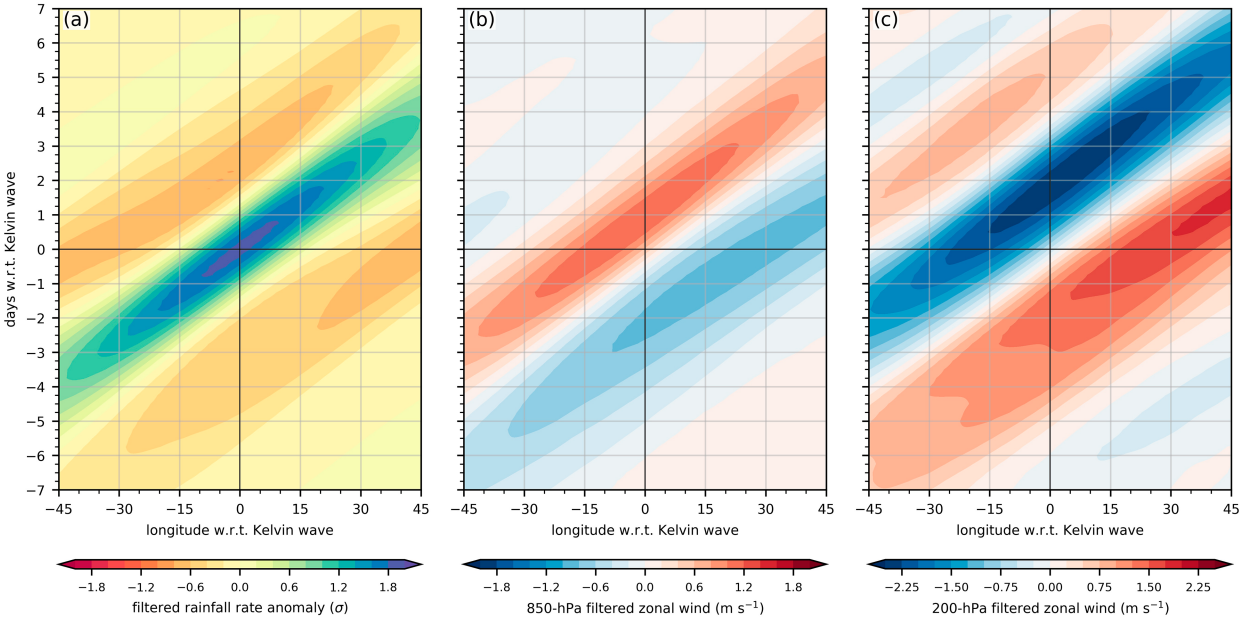

FIG. 2. Hovmöller diagrams of composite filtered (a) rainfall rate, (b) 850-hPa zonal wind, and (c) 200-hPa zonal wind. Longitude and time are shifted with respect to each Kelvin wave rainfall peak.

we tested a second method that combines spatiotemporal filtering with a spatial projection of winds and geopotential height onto the theoretical structure of the waves (Yang et al. 2003). The projection is done via a combination of parabolic cylinder functions (PCF) with a trapping scale of 6° latitude. If the waves identified by spatiotemporal filtering alone are indeed Kelvin waves, we would expect the PCF method to yield filtered winds corresponding to the theoretical structure of Kelvin waves. For this purpose, Fig. 2 shows wave-relative Hovmöller diagrams of filtered rainfall rates and filtered winds at 850 and 200 hPa. We obtained the filtered rainfall rates using only spatiotemporal filtering as described above, whereas we retrieve the filtered winds using the PCF method with a broad window of eastward wavenumbers 1–20 and time periods of 2.5–30 days. To construct the composites, Kelvin wave peaks were identified by calculating maxima in filtered rainfall rate exceeding one standard deviation at each longitude.

The filtered rainfall and wind anomalies are consistent with the expected structure of Kelvin waves. A positive rainfall anomaly propagates eastward with an approximate wavelength (from valley to valley) of 75° or 8325 km and a time period of 6 days (Fig. 2a). These values yield an approximate propagation speed of 15 m s^{-1}, which is within the observed propagation speeds of Kelvin waves (Kiladis et al. 2009). Furthermore, the filtered winds obtained from the PCF projection show the expected structure of Kelvin waves (Figs. 2b,c). Lower-tropospheric easterlies happen to the east or ahead of the Kelvin waves, while lower-tropospheric westerlies happen within and to the west of the rainfall peak (Fig. 2b). An opposite pattern exists in the upper troposphere where westerlies appear to the east or ahead of the wave peak and easterlies appear to the west and behind the wave crest (Fig. 2c). This analysis proves that spatiotemporal filtering is adequate at identifying Kelvin waves in our simulation. The interested reader is referred to RDM23 for more details about the three-dimensional structure of the Kelvin waves.

c. *Tropical cyclone tracking*

We identified and tracked tropical cyclones using the TRACK algorithm (Hodges 1996, 1999; Hodges et al. 2017), which uses spectrally filtered vorticity to determine the presence and lifetime of tropical cyclones. A detailed discussion about the tropical cyclone tracking was provided by RDM23. In short, TRACK identified a tropical cyclone if a lower-tropospheric vorticity anomaly on a T63 spectral grid exceeded 1×10^{-5} s^{-1} for at least 48 h. TRACK also ensured that the anomaly was associated with a warm core (defined as a positive difference between 850- and 200-hPa vorticity) and a vertically coherent vortex (defined as vorticity exceeding 1×10^{-5} s^{-1} at 850, 700, 600, 500, and 200 hPa). We then used a postprocessing algorithm to refine the tropical cyclone tracks and intensity using the native (i.e., 3-km cell spacing) model output.

d. *Determination of TCG–wave lag*

We investigated the relationship between tropical cyclogenesis and Kelvin waves by calculating the time lag between a cyclogenesis event and Kelvin wave crest passing the longitude of cyclogenesis, closely following the steps of Schreck (2015). As discussed in RDM23, cyclogenesis was defined as a 24-h window when the minimum sea level pressure was decreasing and/or a closed isobar existed at the end of the 24-h window. The "genesis time" was taken as the final time of the 24-h window.

Our analysis is centered around the time lag between genesis time and a Kelvin wave. We found Kelvin wave *crests* by obtaining local maxima of filtered rainfall rates that exceeded one standard deviation. We then found the closest Kelvin wave crest to the time and location of cyclogenesis by minimizing a cost function that considered both the location and propagation speed of the Kelvin wave crests. This method is slightly modified from Schreck (2015). We also considered an alternative method that considered the convectively active *phase* of Kelvin waves by constructing a wave phase given by the filtered rainfall rates and their tendencies (Rios-Berrios et al. 2023b, their Fig. 1). However, this method yields very similar results to the method employed here and, therefore, we do not discuss it.

We constructed histograms of the time lag between genesis time and the Kelvin wave crest. As in Schreck (2015), the histograms used 1-day bins where the central time is t_0, and the times considered in each bin spanned $[t_0 - 0.5 \text{ day}, t_0 + 0.5 \text{ day})$. We tested the results for statistical significance by calculating the 99th percentile confidence bounds as outlined by Schreck (2015). The statistical significance test uses the cumulative density function from a binomial distribution to estimate the nth percentages (1% and 99% in our case) of a distribution with N number of samples and a probability p of occurrence. As in Schreck (2015), N was mean of the number of cases within the distribution and p was given by the inverse of the bin width.

e. *Ventilation index*

We calculated the ventilation index using 6-hourly interpolated output between 0° and 20°N, following closely the steps outlined in Tang and Emanuel (2012). The ventilation index Λ is defined as

$$\Lambda = \frac{u_{\text{shear}}}{u_{\text{PI}}}\chi, \tag{1}$$

where u_{shear} is the 200–850-hPa vertical wind shear magnitude, u_{PI} is the maximum potential intensity measured in wind speed (Bister and Emanuel 2002), and χ is the nondimensional entropy deficit. We removed all tropical cyclone circulations following Galarneau and Davis (2013) prior to the calculation of u_{shear}. The u_{PI} is a theoretical maximum intensity that a TC can reach given its environment as measured by a thermodynamic profile and the underlying SST (Emanuel 1986). We calculated u_{PI} following Bister and Emanuel (2002). Tang and Emanuel (2012) defined χ as

$$\chi = \frac{s_m^* - s_m}{s_{\text{SST}}^* - s_b},$$

where s is the pseudoadiabatic moist entropy (Bryan 2008), s_m^* is the saturation moist entropy averaged between 550 and 650 hPa, s_m is the moist entropy over the same layer, s_{SST}^* is the saturation moist entropy at the surface, and s_b is the boundary layer moist entropy. This quantity is a ratio between the entropy deficit of a tropical cyclone with respect to its environment and the air–sea entropy disequilibrium.

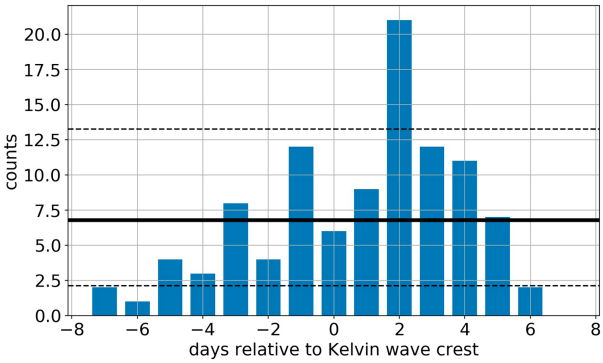

FIG. 3. Histograms of the time lag between tropical cyclogenesis and days relative to a Kelvin wave peak. The solid line represents the mean number of cyclogenesis at all lead times from −8 to +8 days, whereas the dashed lines show the 1st and 99th percentile confidence bounds.

3. Modulation of tropical cyclogenesis by Kelvin waves

Our analysis reveals that Kelvin waves modulate the likelihood of tropical cyclogenesis in the MPAS-A aquaplanet simulation. Histograms of the time lag between a Kelvin wave and tropical cyclogenesis at the same longitude show a prominent and statistically significant peak at 2 days (Fig. 3). The number of tropical cyclogenesis events 2 days after a Kelvin wave peak is at least 2 times as large as the number of events at any other time lag. However, tropical cyclogenesis events happen at any day between 8 days before and 7 days after a Kelvin wave. This result implies that Kelvin waves are not the sole modulators of tropical cyclogenesis; instead, Kelvin waves accelerate or "boost" the processes leading to tropical cyclone formation.

Nonetheless, the modulation is consistent with previous studies that found enhanced tropical cyclogenesis after a Kelvin wave (Ventrice et al. 2012a; Schreck 2015; Lawton and Majumdar 2023). Note that our distributions show a drop-off in counts away from the maximum, whereas the distributions in Schreck (2015) do not show such drop-off. Schreck (2015) considered all wave peaks near the location of tropical cyclogenesis, whereas we only consider the closest wave in time and space.

4. Modulation of synoptic-scale conditions preceding cyclogenesis

With evidence that Kelvin waves modulate tropical cyclogenesis in our aquaplanet simulation, we now explore the mechanisms that explain the higher likelihood of genesis following the passage of these waves. For this purpose, we will focus on 33 cyclogenesis events that occurred between 1.5 and 3.5 days after a Kelvin wave. Despite the relatively short simulation, the number of events is similar to climatological studies using observations (Schreck 2015; Lawton and Majumdar 2023). Figure 4 shows composites of anomalous 850-hPa relative vorticity, rainfall rates, and winds at 850 and 200 hPa for those 33 events. We obtained

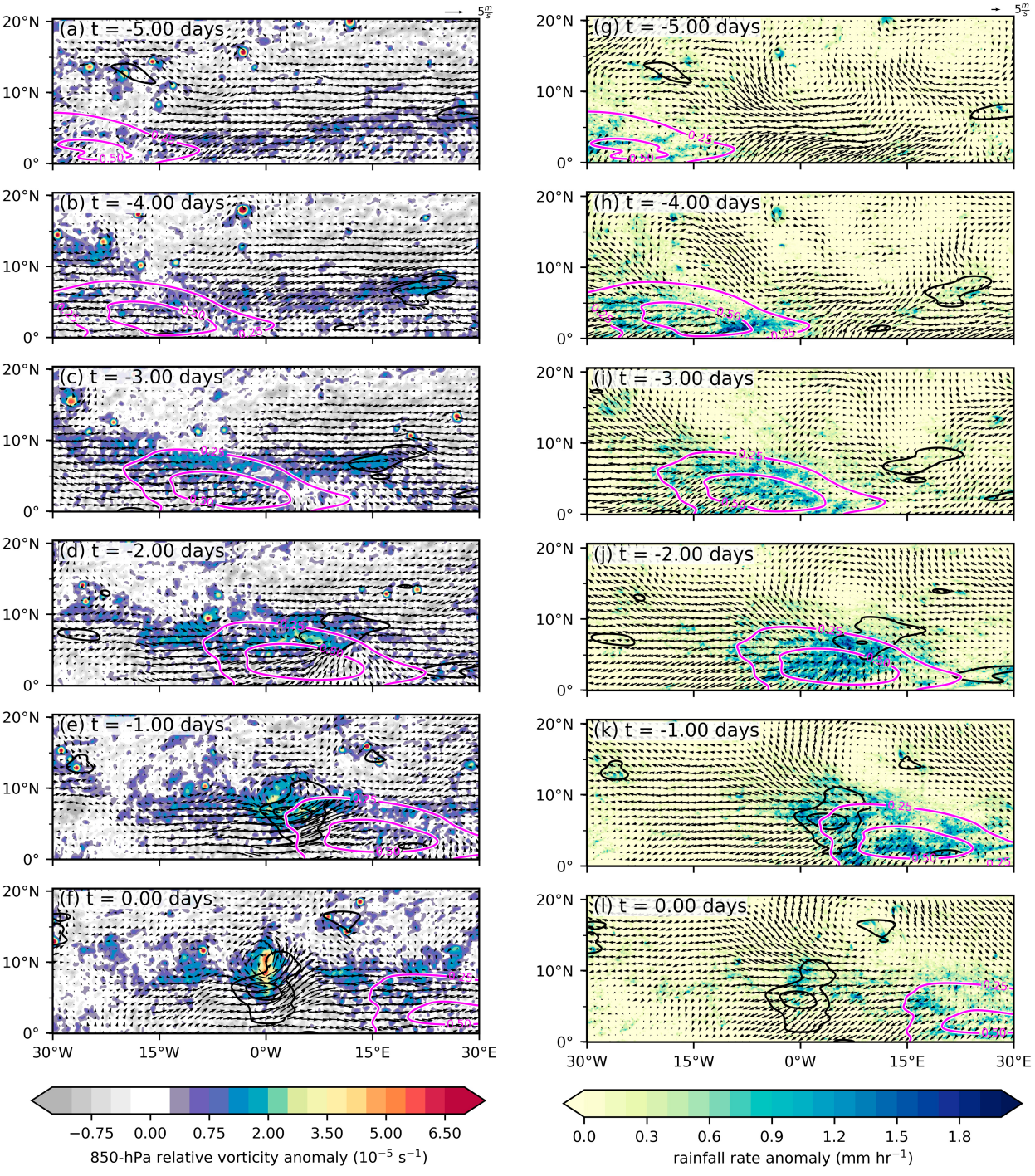

FIG. 4. Time-lagged composites of anomalous (left) 850-hPa relative vorticity (shading) and 850-hPa winds and (right) rainfall rate (shading) and 200-hPa winds. Kelvin and easterly wave–filtered rainfall rates are depicted by the pink and black contours, respectively. Longitude and time are centered on the location and time of tropical cyclogenesis. All anomalies are calculated with respect to time-mean, zonal-mean fields.

anomalies by subtracting the time-mean, zonal-mean conditions of fields centered on the longitude of cyclogenesis for each event. The composites are shifted in longitude, such that 0° represents the longitude where each tropical cyclone forms. Easterly wave–filtered rainfall rates are also shown in Fig. 4 because the pregenesis disturbances project onto the wavenumbers and periods of easterly waves (RDM23).

The composite maps show substantial changes, associated with Kelvin waves, during the week preceding tropical cyclogenesis. Five days before cyclogenesis, anomalous lower-tropospheric easterlies and upper-tropospheric westerlies exist over most of the region where cyclogenesis happens later on (Figs. 4a,g). Anomalous lower-tropospheric cyclonic vorticity is also evident, which is indicative of rotating disturbances within the ITCZ. Convective activity is limited as indicated by negligible rainfall anomalies. As the Kelvin wave travels eastward, anomalous lower-tropospheric cyclonic vorticity and convective activity increase in coverage and magnitude. These changes are especially evident from 4 to 3 days before tropical cyclogenesis (Figs. 4b,c,h,i). A disturbance appears to be organizing and traveling westward toward 15° longitude to the east of the cyclogenesis location (Fig. 4c).

Two days before cyclogenesis, there is a substantial enhancement of lower-tropospheric vorticity anomalies and the associated convective activity (Figs. 4d,j). The Kelvin wave rainfall envelope overlaps with the easterly wave that ultimately becomes a tropical cyclone. The lower-tropospheric flow begins to exhibit more rotation, and the upper-tropospheric flow becomes more divergent. As the Kelvin wave continues propagating eastward, the pregenesis disturbance continues to organize and increase its rotation as indicated by the more concentrated and stronger vorticity and rainfall anomalies 1 day before cyclogenesis (Figs. 4e,k). On the day of cyclogenesis, lower-tropospheric rotating flow and upper-tropospheric divergent flow are clearly evident (Figs. 4f,l). Predominantly lower-tropospheric westerly flow surrounds the tropical cyclone to the south. The region of anomalous convective activity is limited to the tropical cyclone and its near environment, while its surroundings are characterized by relatively low to no convective activity.

This evolution suggests that the passage of the Kelvin wave is critical for both synoptic-scale and mesoscale conditions preceding cyclogenesis. There is a substantial change from relatively unfavorable conditions—characterized by scattered cyclonic vorticity anomalies and low convective activity—to conditions that favor convective organization and vorticity spinup. Consistent with previous studies (Ventrice and Thorncroft 2013; Schreck 2015), cyclogenesis happens in conjunction with anomalous lower-tropospheric westerlies associated with the convectively suppressed phase of the Kelvin wave. This anomalous flow could help enhance the lower-tropospheric vorticity and reduce the vertical wind shear magnitude given the background westerly shear in our simulation (RDM23).

We tested the hypothesis that Kelvin waves modulate the necessary synoptic-scale conditions for tropical cyclogenesis by examining the ventilation index and its components. As discussed earlier, the ventilation index is a theory-based quantity that considers both thermodynamic and kinematic environmental influences on tropical cyclogenesis. This index can be calculated on synoptic time scales unlike other indices that require monthly or seasonal climatologies (such as genesis potential index; Camargo et al. 2007; Emanuel and Nolan 2004; Camargo et al. 2009; Rappin et al. 2010; Camargo et al. 2014). Moreover, the distribution of the ventilation index for developing tropical cyclones in our simulation (Fig. S1) is skewed toward smaller values than climatology as is expected from nature (Tang and Emanuel 2012). The ventilation index is, therefore, a useful metric to characterize the synoptic-scale conditions preceding tropical cyclogenesis in our simulation.

The ventilation index confirms that Kelvin waves modulate the synoptic-scale conditions preceding tropical cyclogenesis. This result is shown in Fig. 5a through a Hovmöller diagram of ventilation index anomalies averaged between 0° and 15°N. Although the Kelvin wave rainfall extends south of the equator (Fig. 4), we focus on the latitudinal band where most tropical cyclones form. By simply considering anomalies with respect to the time- and zonal-mean conditions, the Hovmöller diagram shows an eastward-propagating wave-like signature. Anomalously strong ventilation exists before and to the east of the Kelvin wave rainfall envelope, while anomalously weak ventilation appears during, after, and to the west of the Kelvin wave rainfall envelope. The anomalously weak ventilation appears within a broad region from at least 15°W to 15°E of the location of cyclogenesis. Importantly, these favorable conditions appear and persist from 3 days before to up to a day after cyclogenesis.

Examining the individual components of the ventilation index helps explain the more favorable synoptic-scale conditions after a Kelvin wave (Figs. 5b–d). All three components—χ, u_{shear}, and u_{PI}—exhibit an eastward-propagating wave-like pattern with the more favorable conditions happening during and after the Kelvin wave rainfall envelope. Specifically, anomalously moist air (i.e., low χ), anomalously weak shear, and anomalously high u_{PI} all follow the Kelvin wave. In contrast, less favorable conditions appear before and to the east of the Kelvin wave. There is a lag between χ and u_{shear} such that anomalously moist conditions appear first followed by anomalously weak shear. These results show that Kelvin waves provide favorable synoptic-scale conditions not only due to their perturbations to the kinematic conditions but also due to thermodynamic factors.

To further explore the relative role of each of the components of the ventilation index, we applied the natural logarithm to Eq. (1), which yields

$$\ln(\Lambda) = \ln(\chi) + \ln(u_{\text{shear}}) - \ln(u_{\text{PI}}). \tag{2}$$

We then examined the relative changes of each component by taking a differential on each side:

$$\delta\ln(\Lambda) = \delta\ln(\chi) + \delta\ln(u_{\text{shear}}) - \delta\ln(u_{\text{PI}}). \tag{3}$$

By definition,

$$\delta\ln(x) = \frac{x_0 - x}{x},$$

where x is a variable of interest (Λ, χ, u_{shear}, or u_{PI} in our case) and the subscript 0 represents a reference point in time and space. This method allows us to quantify the relative changes of each term and their relative contributions to the ventilation index. For our purposes, we evaluated x_0 at the time of cyclogenesis and x 5 days before to investigate the changes in environmental conditions leading to cyclogenesis

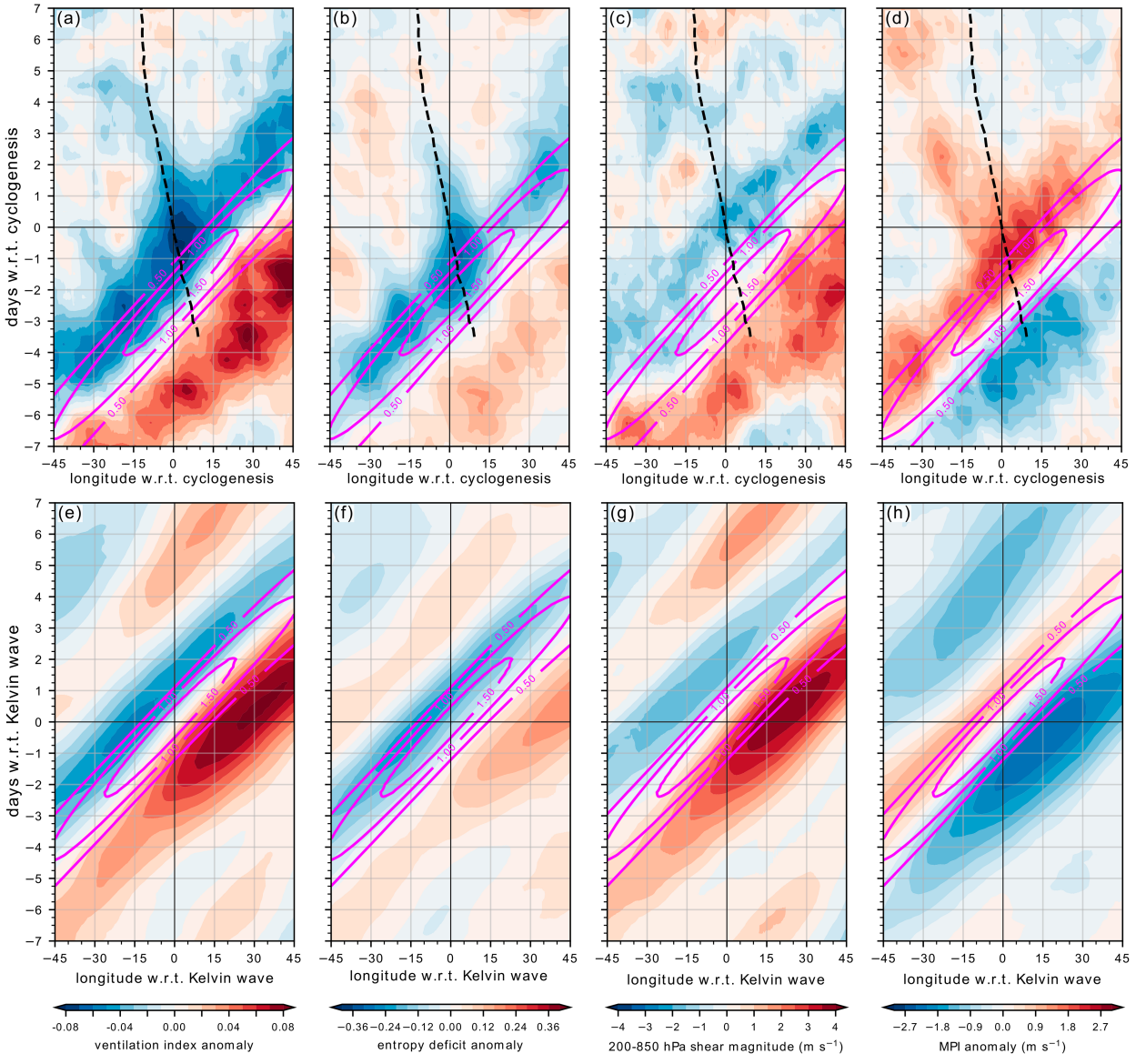

FIG. 5. Hovmöller diagrams of composite (a),(e) ventilation index, (b),(f) entropy deficit, (c),(g) 200–850-hPa vertical wind shear magnitude, and (d),(h) maximum potential intensity anomalies. Magenta contours depict the filtered Kelvin wave rainfall rate anomalies (every 0.5 mm h^{-1}). In (a)–(d), composites are centered on the longitude and time of tropical cyclogenesis; dashed lines depict the average tropical disturbance/cyclone location. In (e) and (f), composites are centered on the longitude and time of Kelvin wave peaks.

(Figs. 4 and 5). Figure 6 shows all terms of Eq. (3) evaluated between 0° and 15°N. As a final step, we calculated the fractional contribution (FC) (Andersen and Kuang 2012; Arnold et al. 2015; Wolding et al. 2020) from each term to the total ventilation index changes as follows:

$$\mathrm{FC} = \frac{\sum_{j=0}^{N} \delta\ln(\Lambda)_j \delta\ln(x)_j}{\sum_{j=0}^{N} \delta\ln(x)_j \delta\ln(x)_j},$$

where x is χ, u_{shear}, or u_{PI} and j is an individual point.

This analysis provides quantitative evidence that thermodynamics, not just kinematics, influence the environmental conditions associated with Kelvin waves and their modulation of tropical cyclogenesis. Figure 6a shows a reduction of ventilation index from approximately 10°W to 40°E of the location of cyclogenesis. The reduction is asymmetric—most of the reduction happens to the east of the cyclogenesis location where westward-moving pregenesis disturbances form and evolve (Fig. 4). Examining the components of the ventilation index shows that χ is the major contributor to the ventilation reduction (Fig. 6a). The changes in the ventilation index largely follow the changes of χ, and the magnitude of the χ changes is

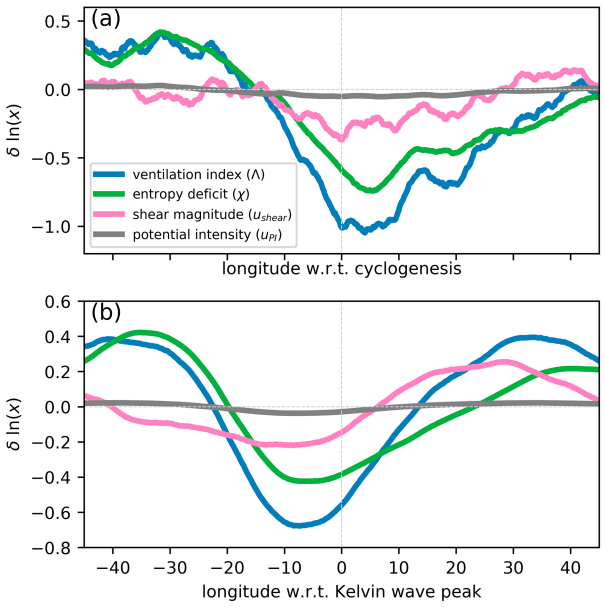

FIG. 6. Temporal changes of latitudinally averaged (blue) ventilation index, (green) entropy deficit, (pink), vertical wind shear magnitude, and (gray) maximum potential intensity. (a) Changes calculated between 5 days before and the day of *cyclogenesis* and averaged 0°–15°N. (b) Changes calculated between 2 days and the day of *a Kelvin wave peak*.

more than half the magnitude of the ventilation changes. The FC from changes in χ is 0.73. The magnitude of vertical wind shear also decreases during the 5 days leading to cyclogenesis and contributes to the ventilation reduction, but its changes are much smaller than the moist entropy changes. The FC from changes in u_{shear} is 0.21—less than a third the FC from χ. Shear magnitude seems to play a secondary yet important role. Last, the changes in potential intensity are nearly negligible (FC of 0.06).

Our analysis so far suggests that Kelvin waves modulate key synoptic-scale factors that are necessary yet insufficient for tropical cyclogenesis; however, there are several limitations to these results. First, the sample size is relatively small (33 cases). A longer simulation would be needed to confirm our results with a larger sample size. Second, the process of cyclogenesis itself may contribute to some of the noted changes in the ventilation index and its components. For example, Figs. 5a and 5b show a broad and westward-propagating anomaly (between 0° and 15°W, −1 to 2 days) associated with the developing tropical cyclones. The next section will address these limitations.

5. Modulation of synoptic-scale conditions by Kelvin waves

We aim at confirming and explaining the findings of the previous section with an analysis of Kelvin waves regardless of whether they were followed by a cyclogenesis event. To this end, we repeated the analysis of the ventilation index and its components with respect to Kelvin wave peaks that we identified from the filtered wave rainfall rates. We excluded any wave peaks that coincided with hurricane-strength tropical cyclones within 45° longitude to the east and west and within 7 days before and after the wave peaks (i.e., the domains of Figs. 5e–h). After this exclusion, we identified 1734 individual Kelvin wave peaks. By considering over a thousand samples, we can examine anomalous fields that are most likely associated with and attributable to Kelvin waves.

This analysis confirms that Kelvin waves modulate synoptic-scale conditions that are important for tropical cyclogenesis. Kelvin wave-relative composites of the ventilation index and all of its components show an eastward-propagating wave-like signature (Figs. 5e–h). The wave-like pattern follows very closely the filtered rainfall anomalies associated with Kelvin waves. Anomalously weak ventilation appears within and to the west of (or behind) the Kelvin wave rainfall envelope, while anomalously strong ventilation appears to the east of (or ahead) the waves (Fig. 5e). Consistent with this pattern, anomalously weak χ (Fig. 5f), anomalously weak u_{shear} (Fig. 5g), and anomalously strong u_{PI} (Fig. 5h) appear within and to the west of (or behind) the Kelvin wave rainfall envelope. These conditions could support convective organization and the establishment of a vertically coherent vortex, given the smaller degree (than background conditions) of cool, dry air being imported from the environment into a disturbance. Opposite anomalies appear to the east of (or ahead) the Kelvin waves.

We now quantify the changes in the ventilation index and its components leading to the day of the Kelvin wave rainfall peak. We evaluated Eq. (3) 2 days before and on the day of the Kelvin wave peak with the intention of quantifying the changes seen in Fig. 5e. This analysis shows a substantial ventilation decrease during 2 days leading up to the Kelvin wave crest (Fig. 6b). The peak magnitude of the change is about 0.6, indicating a reduction in the ventilation index by nearly 60%. Importantly, the pattern of the change is asymmetric in longitude with the largest changes happening between 25° to the west and 15° to the east of the Kelvin wave crest. This asymmetric pattern provides an additional explanation for the increased likelihood of tropical cyclogenesis after the passage of a Kelvin wave—a pregenesis, westward-moving disturbance would have an extensive region of anomalously favorable synoptic conditions.

Examining the changes of individual components confirms that most of the ventilation changes happen due to χ with u_{shear} playing a secondary role (Fig. 6b). There is a substantial reduction in χ between 20° to the west and 20° to the east of the Kelvin wave peak, with the maximum change happening approximately 5° west of the wave crest. Likewise, an increase in χ is evident westward of 20° west and eastward of 20° east of the Kelvin wave crest. The FC from χ changes to ventilation changes is 0.66. In contrast, the FC due to vertical wind shear and potential intensity is 0.28 and 0.05, respectively. The u_{PI} plays little to no role, likely because the background u_{PI} depends on the time-fixed, zonally symmetric SST of our simulation. This variable may be more important in nature.

A novel finding here is the modulation of χ by the Kelvin waves, which can be explained by their vertically tilted thermodynamic structure. This result is shown in Fig. 7 through vertical cross sections centered on the Kelvin wave peaks. A positive anomaly, vertically tilted from east to west, is evident in the pseudoadiabatic moist entropy (Fig. 7a). Peak positive anomalies appear between 300–600 hPa and 5°–20° to the west of the Kelvin wave crest. These positive anomalies are associated with positive anomalies of both temperature *and* water vapor mixing ratio—peak warm anomalies appear between 200 and 400 hPa (Fig. 7b), while peak moist anomalies appear between 400 and 600 hPa (Fig. 7c). Importantly, negative moist entropy anomalies exist in the lower troposphere below the positive moist entropy anomalies to the west of the Kelvin wave crest (Fig. 7a). With zonally symmetric SSTs, the negative anomalies yield a larger air–sea disequilibrium westward of the Kelvin wave peak. The χ is a ratio of the saturation deficit of the middle troposphere to the air–sea moist entropy disequilibrium. Hence, the weaker and more favorable χ stems from a combination of a warmer and wetter middle troposphere together with a cooler and drier boundary layer. These results stress the importance of the vertical tilt of both temperature and water vapor in modulating the synoptic-scale thermodynamic conditions for tropical cyclogenesis.

6. Summary and discussion

This study analyzes the modulation of tropical cyclogenesis by convectively coupled Kelvin waves in a convection-permitting aquaplanet simulation. Results confirm a time-lagged relationship between the passage of a Kelvin wave crest and an increased likelihood of tropical cyclogenesis. A statistically significant enhancement of tropical cyclogenesis appears 2 days *after* a Kelvin wave crest. This result is consistent with previous studies that relied on reanalysis, best tracks, and satellite data, thus suggesting that the aquaplanet simulation captures the key factors and processes that explain the Kelvin wave–tropical cyclogenesis relationship. This study focused on understanding the synoptic-scale factors that explain the tropical cyclogenesis modulation by Kelvin waves, while a future study should focus on the mesoscale and convective-scale processes. Figure 8 highlights the key factors and processes identified in this study, which are also summarized below.

Our results demonstrate that Kelvin waves modulate key synoptic-scale conditions that are necessary for tropical cyclogenesis. We diagnosed those conditions primarily using the ventilation index—a theory-based index that has been shown to distinguish between favorable and nonfavorable environments for tropical cyclogenesis (Tang and Emanuel 2012). Composites of ventilation index anomalies with respect to tropical cyclogenesis show an eastward-propagating wave-like signature following the Kelvin wave rainfall envelope. Anomalously small and favorable ventilation index values exist during and to the west of (or behind) the Kelvin wave, which coincides with 2–4 days prior to cyclogenesis. The anomalously small ventilation is influenced foremost by anomalously low entropy deficit (i.e., anomalously moist midtropospheric conditions), next by weak vertical wind shear, and only to a small degree by high maximum potential intensity. Pregenesis disturbances, most likely associated with easterly waves (see RDM23), likely benefit from those expansive favorable conditions to develop into tropical cyclones.

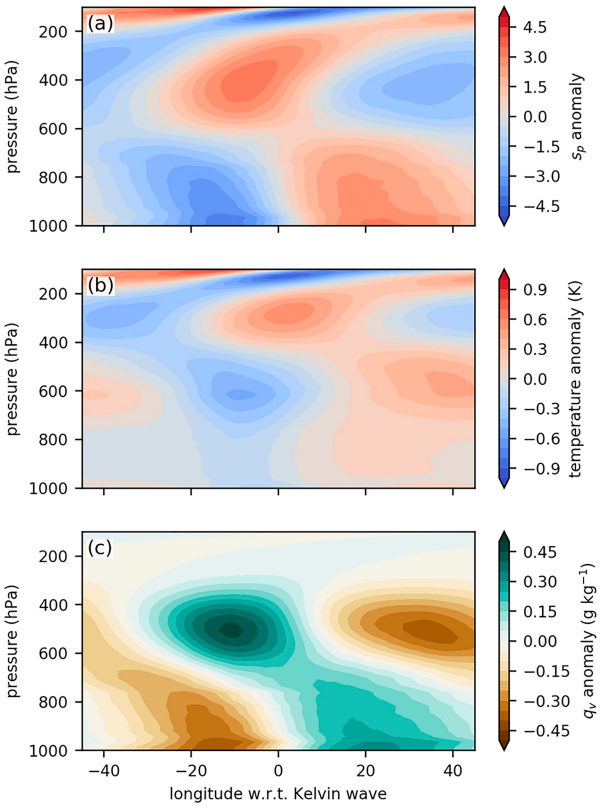

FIG. 7. Vertical cross sections of 0°–15°N latitudinally averaged (a) pseudoadiabatic moist entropy, (b) temperature, and (c) specific humidity composite anomalies associated with Kelvin waves. The longitude axis is centered on the location of Kelvin wave peaks.

Composites relative to Kelvin waves—excluding hurricane-strength tropical cyclones—confirm that these waves indeed modulate the ventilation index, its components, and other important factors for tropical cyclogenesis. The anomalously low entropy deficit results from the vertically tilted moisture and temperature structure associated with Kelvin waves. Moreover, temporal changes in the ventilation index are dominated by changes in the entropy deficit, followed by changes in vertical wind shear. The temporal and spatial lag between ventilation and shear leads us to hypothesize that Kelvin waves may facilitate tropical cyclogenesis by first promoting convective activity and suppressing mesoscale downdrafts (Bister and Emanuel 1997), followed by the development of a vertically aligned vortex and continued convective organization under relatively weak shear (Davis and Ahijevych 2012). These processes are associated with a 2-day lag, which also corresponds to the approximate time scale of tropical cyclogenesis from a preexisting disturbance in our simulation.

This study opens up opportunities for future research. We use an idealized framework as a "clean" laboratory that allows us to focus on Kelvin waves and tropical cyclones.

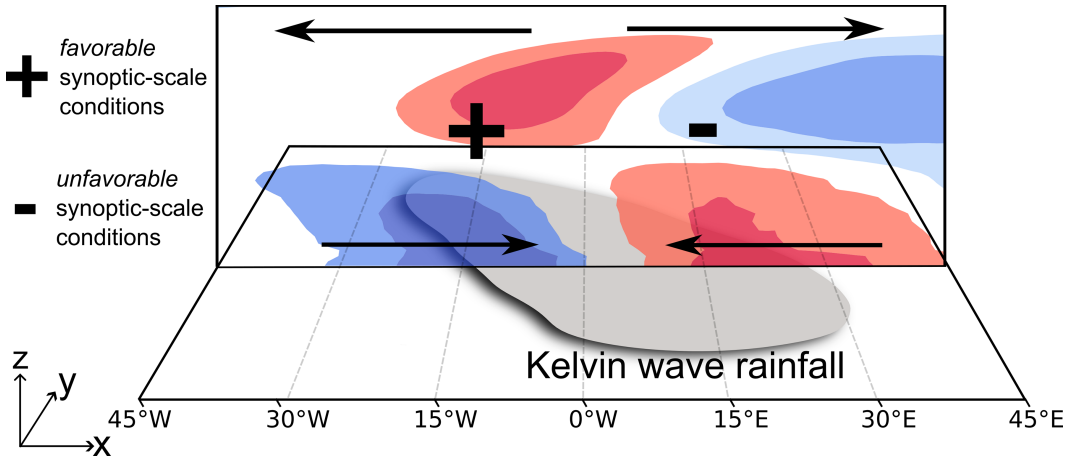

FIG. 8. Three-dimensional summary schematic of the key factors identified in this study. The gray shading represents the Kelvin wave rainfall, whereas the red and blue shadings represent the moist entropy anomalies (red for positive anomalies; blue for negative anomalies). The arrows represent the anomalous winds. The Kelvin wave rainfall is on the x–y plane; the moist entropy is on the x–z plane. Last, the plus (+) and minus (−) signs indicate the regions of favorable and unfavorable, respectively, synoptic-scale conditions for tropical cyclogenesis during a Kelvin wave passage.

However, this framework excludes many real-world factors (e.g., subseasonal ocean variability, basin geometries, and topography) that may be important for tropical cyclogenesis. We hypothesize that our results most likely apply to the east Pacific basin, where the aquaplanet is most similar to Earth (RDM23) and where the relationship between Kelvin waves and tropical cyclogenesis is strongest (Schreck 2015, 2016). We stress that our results are based on a single idealized simulation of the tropical atmosphere. While the Kelvin waves in this simulation resemble their observed counterparts (RDM23), there is no observational evidence available to confirm how Kelvin waves modulate ventilation. An analysis of the ventilation index and its components using reanalysis or sounding data is needed to confirm that our results also apply to Kelvin waves in nature. Additionally, our simulation had no MJO, which is a known modulator of planetary-scale and synoptic-scale conditions. A future study should evaluate whether the results found herein also apply to the documented modulation of tropical cyclogenesis by the MJO (Frank and Roundy 2006; Maloney and Hartmann 2000a,b; Bessafi and Wheeler 2006; Klotzbach 2010; Klotzbach and Oliver 2014, 2015). The MJO is also associated with vertically tilted temperature and moist anomalies (Adames and Wallace 2015) that could promote low entropy deficit over larger spatial and temporal scales than Kelvin waves. Last, a verification study is needed to investigate if numerical models used for subseasonal prediction can realistically capture Kelvin waves, their modulation of synoptic-scale conditions, and their relationship with tropical cyclogenesis.

Acknowledgments. We thank Drs. George Bryan, Falko Judt, Rich Rotunno, Kerry Emanuel, Paul Roundy, George Kiladis, and Carl Schreck for helpful discussions that helped improve this research. We also thank NSF NCAR's Computational Information Systems Laboratory for their supercomputing and data support with the Cheyenne supercomputing system (https://doi.org/10.5065/D6RX99HX). This work is based upon work supported by NSF NCAR, which is a major facility sponsored by the National Science Foundation under Cooperative Agreement 1852977.

Data availability statement. The interpolated model output used in this study is publicly and freely available to the research community (Rios-Berrios 2023). The native model output is also freely available and can be disseminated upon request due to its large volume.

REFERENCES

Adames, Á. F., and J. M. Wallace, 2015: Three-dimensional structure and evolution of the moisture field in the MJO. *J. Atmos. Sci.*, **72**, 3733–3754, https://doi.org/10.1175/JAS-D-15-0003.1.

Alland, J. J., B. H. Tang, K. L. Corbosiero, and G. H. Bryan, 2021a: Combined effects of midlevel dry air and vertical wind shear on tropical cyclone development. Part I: Downdraft ventilation. *J. Atmos. Sci.*, **78**, 763–782, https://doi.org/10.1175/JAS-D-20-0054.1.

——, ——, ——, and ——, 2021b: Combined effects of midlevel dry air and vertical wind shear on tropical cyclone development. Part II: Radial ventilation. *J. Atmos. Sci.*, **78**, 783–796, https://doi.org/10.1175/JAS-D-20-0055.1.

Andersen, J. A., and Z. Kuang, 2012: Moist static energy budget of MJO-like disturbances in the atmosphere of a zonally symmetric aquaplanet. *J. Climate*, **25**, 2782–2804, https://doi.org/10.1175/JCLI-D-11-00168.1.

Arnold, N. P., M. Branson, Z. Kuang, D. A. Randall, and E. Tziperman, 2015: MJO intensification with warming in the superparameterized CESM. *J. Climate*, **28**, 2706–2724, https://doi.org/10.1175/JCLI-D-14-00494.1.

Ballinger, A. P., T. M. Merlis, I. M. Held, and M. Zhao, 2015: The sensitivity of tropical cyclone activity to off-equatorial thermal forcing in aquaplanet simulations. *J. Atmos. Sci.*, **72**, 2286–2302, https://doi.org/10.1175/JAS-D-14-0284.1.

Bessafi, M., and M. C. Wheeler, 2006: Modulation of South Indian Ocean tropical cyclones by the Madden–Julian oscillation and convectively coupled equatorial waves. *Mon. Wea. Rev.*, **134**, 638–656, https://doi.org/10.1175/MWR3087.1.

Bister, M., and K. A. Emanuel, 1997: The genesis of Hurricane Guillermo: TEXMEX analyses and a modeling study. *Mon. Wea. Rev.*, **125**, 2662–2682, https://doi.org/10.1175/1520-0493(1997)125<2662:TGOHGT>2.0.CO;2.

——, and ——, 2002: Low frequency variability of tropical cyclone potential intensity 1. Interannual to interdecadal variability. *J. Geophys. Res.*, **107**, 4801, https://doi.org/10.1029/2001JD000776.

Blackburn, M., and Coauthors, 2013: The Aqua-Planet Experiment (APE): CONTROL SST simulation. *J. Meteor. Soc. Japan*, **91A**, 17–56, https://doi.org/10.2151/jmsj.2013-A02.

Bryan, G. H., 2008: On the computation of pseudoadiabatic entropy and equivalent potential temperature. *Mon. Wea. Rev.*, **136**, 5239–5245, https://doi.org/10.1175/2008MWR2593.1.

Camargo, S. J., A. H. Sobel, A. G. Barnston, and K. A. Emanuel, 2007: Tropical cyclone genesis potential index in climate models. *Tellus*, **59A**, 428–443, https://doi.org/10.1111/j.1600-0870.2007.00238.x.

——, M. C. Wheeler, and A. H. Sobel, 2009: Diagnosis of the MJO modulation of tropical cyclogenesis using an empirical index. *J. Atmos. Sci.*, **66**, 3061–3074, https://doi.org/10.1175/2009JAS3101.1.

——, M. K. Tippett, A. H. Sobel, G. A. Vecchi, and M. Zhao, 2014: Testing the performance of tropical cyclone genesis indices in future climates using the HiRAM model. *J. Climate*, **27**, 9171–9196, https://doi.org/10.1175/JCLI-D-13-00505.1.

Computational and Information Systems Laboratory, 2023: Cheyenne: HPE/SGI ICE XA system (NCAR community computing), Boulder, CO. National Center for Atmospheric Research, https://doi.org/10.5065/D6RX99HX.

Davis, C. A., and D. A. Ahijevych, 2012: Mesoscale structural evolution of three tropical weather systems observed during PREDICT. *J. Atmos. Sci.*, **69**, 1284–1305, https://doi.org/10.1175/JAS-D-11-0225.1.

Emanuel, K. A., 1986: An air-sea interaction theory for tropical cyclones. Part I: Steady-state maintenance. *J. Atmos. Sci.*, **43**, 585–605, https://doi.org/10.1175/1520-0469(1986)043<0585:AASITF>2.0.CO;2.

——, and D. S. Nolan, 2004: Tropical cyclone activity and global climate system. *26th Conf. on Hurricanes and Tropical Meteorology*, Miami, FL, Amer. Meteor. Soc., 10A.2, https://ams.confex.com/ams/pdfpapers/75463.pdf.

Feng, X., G.-Y. Yang, K. I. Hodges, and J. Methven, 2023: Equatorial waves as useful precursors to tropical cyclone occurrence and intensification. *Nat. Commun.*, **14**, 511, https://doi.org/10.1038/s41467-023-36055-5.

Frank, W. M., and P. E. Roundy, 2006: The role of tropical waves in tropical cyclogenesis. *Mon. Wea. Rev.*, **134**, 2397–2417, https://doi.org/10.1175/MWR3204.1.

Galarneau, T. J., Jr., and C. A. Davis, 2013: Diagnosing forecast errors in tropical cyclone motion. *Mon. Wea. Rev.*, **141**, 405–430, https://doi.org/10.1175/MWR-D-12-00071.1.

Ge, X., T. Li, and M. Peng, 2013: Effects of vertical shears and midlevel dry air on tropical cyclone developments. *J. Atmos. Sci.*, **70**, 3859–3875, https://doi.org/10.1175/JAS-D-13-066.1.

Gray, W. M., 1968: Global view of the origin of tropical disturbances and storms. *Mon. Wea. Rev.*, **96**, 669–700, https://doi.org/10.1175/1520-0493(1968)096<0669:GVOTOO>2.0.CO;2.

——, 1979: Hurricanes: Their formation, structure, and likely role in the tropical circulation. *Meteorology over the Tropical Oceans*, D. B. Shaw, Ed., Royal Meteorological Society, 155–218.

Helms, C. N., and R. E. Hart, 2015: The evolution of dropsonde-derived kinematic and thermodynamic structures in developing and nondeveloping Atlantic tropical convective systems. *Mon. Wea. Rev.*, **143**, 3109–3135, https://doi.org/10.1175/MWR-D-14-00242.1.

Hodges, K., A. Cobb, and P. L. Vidale, 2017: How well are tropical cyclones represented in reanalysis datasets? *J. Climate*, **30**, 5243–5264, https://doi.org/10.1175/JCLI-D-16-0557.1.

Hodges, K. I., 1996: Spherical nonparametric estimators applied to the UGAMP model integration for AMIP. *Mon. Wea. Rev.*, **124**, 2914–2932, https://doi.org/10.1175/1520-0493(1996)124<2914:SNEATT>2.0.CO;2.

——, 1999: Adaptive constraints for feature tracking. *Mon. Wea. Rev.*, **127**, 1362–1373, https://doi.org/10.1175/1520-0493(1999)127<1362:ACFFT>2.0.CO;2.

Hong, S.-Y., J. Dudhia, and S.-H. Chen, 2004: A revised approach to ice microphysical processes for the bulk parameterization of clouds and precipitation. *Mon. Wea. Rev.*, **132**, 103–120, https://doi.org/10.1175/1520-0493(2004)132<0103:ARATIM>2.0.CO;2.

——, Y. Noh, and J. Dudhia, 2006: A new vertical diffusion package with an explicit treatment of entrainment processes. *Mon. Wea. Rev.*, **134**, 2318–2341, https://doi.org/10.1175/MWR3199.1.

Iacono, M. J., J. S. Delamere, E. J. Mlawer, M. W. Shephard, S. A. Clough, and W. D. Collins, 2008: Radiative forcing by long-lived greenhouse gases: Calculations with the AER radiative transfer models. *J. Geophys. Res.*, **113**, D13103, https://doi.org/10.1029/2008JD009944.

Kiladis, G. N., M. C. Wheeler, P. T. Haertel, K. H. Straub, and P. E. Roundy, 2009: Convectively coupled equatorial waves. *Rev. Geophys.*, **47**, RG2003, https://doi.org/10.1029/2008RG000266.

Klotzbach, P. J., 2010: On the Madden–Julian oscillation–Atlantic hurricane relationship. *J. Climate*, **23**, 282–293, https://doi.org/10.1175/2009JCLI2978.1.

——, and E. C. J. Oliver, 2014: Modulation of Atlantic basin tropical cyclone activity by the Madden–Julian Oscillation (MJO) from 1905 to 2011. *J. Climate*, **28**, 204–217, https://doi.org/10.1175/JCLI-D-14-00509.1.

——, and ——, 2015: Variations in global tropical cyclone activity and the Madden-Julian Oscillation since the midtwentieth century. *Geophys. Res. Lett.*, **42**, 4199–4207, https://doi.org/10.1002/2015GL063966.

Knippertz, P., and Coauthors, 2022: The intricacies of identifying equatorial waves. *Quart. J. Roy. Meteor. Soc.*, **148**, 2814–2852, https://doi.org/10.1002/qj.4338.

Komaromi, W. A., 2013: An investigation of composite dropsonde profiles for developing and nondeveloping tropical waves during the 2010 PREDICT field campaign. *J. Atmos. Sci.*, **70**, 542–558, https://doi.org/10.1175/JAS-D-12-052.1.

Lawton, Q. A., and S. J. Majumdar, 2023: Convectively coupled Kelvin waves and tropical cyclogenesis: Connections through convection and moisture. *Mon. Wea. Rev.*, **151**, 1647–1666, https://doi.org/10.1175/MWR-D-23-0005.1.

——, ——, K. Dotterer, C. Thorncroft, and C. J. Schreck III, 2022: The influence of convectively coupled Kelvin waves on African easterly waves in a wave-following framework. *Mon. Wea. Rev.*, **150**, 2055–2072, https://doi.org/10.1175/MWR-D-21-0321.1.

Maloney, E. D., and D. L. Hartmann, 2000a: Modulation of eastern North Pacific hurricanes by the Madden–Julian oscillation. *J. Climate*, **13**, 1451–1460, https://doi.org/10.1175/1520-0442(2000)013<1451:MOENPH>2.0.CO;2.

——, and ——, 2000b: Modulation of hurricane activity in the Gulf of Mexico by the Madden-Julian oscillation. *Science*, **287**, 2002–2004, https://doi.org/10.1126/science.287.5460.2002.

Mlawer, E. J., S. J. Taubman, P. D. Brown, M. J. Iacono, and S. A. Clough, 1997: Radiative transfer for inhomogeneous atmospheres: RRTM, a validated correlated-k model for the longwave. *J. Geophys. Res.*, **102**, 16 663–16 682, https://doi.org/10.1029/97JD00237.

Murakami, H., 2014: Tropical cyclones in reanalysis data sets. *Geophys. Res. Lett.*, **41**, 2133–2141, https://doi.org/10.1002/2014GL059519.

Nakamura, Y., and Y. N. Takayabu, 2022: Convective couplings with equatorial Rossby waves and equatorial Kelvin waves. Part I: Coupled wave structures. *J. Atmos. Sci.*, **79**, 247–262, https://doi.org/10.1175/JAS-D-21-0080.1.

Nolan, D. S., 2007: What is the trigger for tropical cyclogenesis? *Aust. Meteor. Mag.*, **56**, 241–266.

——, and E. D. Rappin, 2008: Increased sensitivity of tropical cyclogenesis to wind shear in higher SST environments. *Geophys. Res. Lett.*, **35**, L14805, https://doi.org/10.1029/2008GL034147.

Papin, P. P., L. F. Bosart, and R. D. Torn, 2020: A feature-based approach to classifying summertime potential vorticity streamers linked to Rossby wave breaking in the North Atlantic Basin. *J. Climate*, **33**, 5953–5969, https://doi.org/10.1175/JCLI-D-19-0812.1.

Rappin, E. D., D. S. Nolan, and K. A. Emanuel, 2010: Thermodynamic control of tropical cyclogenesis in environments of radiative-convective equilibrium with shear. *Quart. J. Roy. Meteor. Soc.*, **136**, 1954–1971, https://doi.org/10.1002/qj.706.

Raymond, D. D. J., C. López-Carrillo, and L. L. Cavazos, 1998: Case-studies of developing East Pacific easterly waves. *Quart. J. Roy. Meteor. Soc.*, **124**, 2005–2034, https://doi.org/10.1002/qj.49712455011.

Rios-Berrios, R., 2023: MPAS-A aquaplanet simulation with convection-permitting resolution and off-equatorial SST maximum. UCAR/NCAR – GDEX, https://gdex.ucar.edu/dataset/id/c5755cab-b90d-40a9-b55c-abb90d60a933.html.

——, and R. D. Torn, 2017: Climatological analysis of tropical cyclone intensity changes under moderate vertical wind shear. *Mon. Wea. Rev.*, **145**, 1717–1738, https://doi.org/10.1175/MWR-D-16-0350.1.

——, B. Medeiros, and G. H. Bryan, 2020: Mean climate and tropical rainfall variability in aquaplanet simulations using the model for prediction across scales-atmosphere. *J. Adv. Model. Earth Syst.*, **12**, e2020MS002102, https://doi.org/10.1029/2020MS002102.

——, G. H. Bryan, B. Medeiros, F. Judt, and W. Wang, 2022: Differences in tropical rainfall in aquaplanet simulations with resolved or parameterized deep convection. *J. Adv. Model. Earth Syst.*, **14**, e2021MS002902, https://doi.org/10.1029/2021MS002902.

——, C. A. Davis, and J. Martinez, 2023a: Tropical cyclones and equatorial waves in a convection-permitting aquaplanet simulation with an off-equatorial SST maximum. *J. Adv. Model. Earth Syst.*, **15**, e2023MS003723, https://doi.org/10.1029/2023MS003723.

——, F. Judt, G. Bryan, B. Medeiros, and W. Wang, 2023b: Three-dimensional structure of convectively coupled equatorial waves in aquaplanet experiments with resolved or parameterized convection. *J. Climate*, **36**, 2895–2915, https://doi.org/10.1175/JCLI-D-22-0422.1.

Roundy, P. E., 2008: Analysis of convectively coupled Kelvin waves in the Indian Ocean MJO. *J. Atmos. Sci.*, **65**, 1342–1359, https://doi.org/10.1175/2007JAS2345.1.

——, and W. M. Frank, 2004: A climatology of waves in the equatorial region. *J. Atmos. Sci.*, **61**, 2105–2132, https://doi.org/10.1175/1520-0469(2004)061<2105:ACOWIT>2.0.CO;2.

Schenkel, B. A., and R. E. Hart, 2012: An examination of tropical cyclone position, intensity, and intensity life cycle within atmospheric reanalysis datasets. *J. Climate*, **25**, 3453–3475, https://doi.org/10.1175/2011JCLI4208.1.

Schreck, C. J., III, 2015: Kelvin waves and tropical cyclogenesis: A global survey. *Mon. Wea. Rev.*, **143**, 3996–4011, https://doi.org/10.1175/MWR-D-15-0111.1.

——, 2016: Convectively coupled Kelvin waves and tropical cyclogenesis in a semi-Lagrangian framework. *Mon. Wea. Rev.*, **144**, 4131–4139, https://doi.org/10.1175/MWR-D-16-0237.1.

——, J. Molinari, and K. I. Mohr, 2011: Attributing tropical cyclogenesis to equatorial waves in the western North Pacific. *J. Atmos. Sci.*, **68**, 195–209, https://doi.org/10.1175/2010JAS3396.1.

——, ——, and A. Aiyyer, 2012: A global view of equatorial waves and tropical cyclogenesis. *Mon. Wea. Rev.*, **140**, 774–788, https://doi.org/10.1175/MWR-D-11-00110.1.

Skamarock, W. C., J. B. Klemp, M. G. Duda, L. D. Fowler, S.-H. Park, and T. D. Ringler, 2012: A multiscale nonhydrostatic atmospheric model using centroidal voronoi tesselations and C-grid staggering. *Mon. Wea. Rev.*, **140**, 3090–3105, https://doi.org/10.1175/MWR-D-11-00215.1.

Straub, K. H., and G. N. Kiladis, 2003: The observed structure of convectively coupled Kelvin waves: Comparison with simple models of coupled wave instability. *J. Atmos. Sci.*, **60**, 1655–1668, https://doi.org/10.1175/1520-0469(2003)060<1655:TOSOCC>2.0.CO;2.

Tang, B., and K. Emanuel, 2010: Midlevel ventilation's constraint on tropical cyclone intensity. *J. Atmos. Sci.*, **67**, 1817–1830, https://doi.org/10.1175/2010JAS3318.1.

——, and ——, 2012: A ventilation index for tropical cyclones. *Bull. Amer. Meteor. Soc.*, **93**, 1901–1912, https://doi.org/10.1175/BAMS-D-11-00165.1.

——, and S. J. Camargo, 2014: Environmental control of tropical cyclones in CMIP5: A ventilation perspective. *J. Adv. Model. Earth Syst.*, **6**, 115–128, https://doi.org/10.1002/2013MS000294.

Tao, D., and F. Zhang, 2014: Effect of environmental shear, sea-surface temperature, and ambient moisture on the formation and predictability of tropical cyclones: An ensemble-mean perspective. *J. Adv. Model. Earth Syst.*, **6**, 384–404, https://doi.org/10.1002/2014MS000314.

Vecchi, G. A., and Coauthors, 2019: Tropical cyclone sensitivities to CO_2 doubling: Roles of atmospheric resolution, synoptic variability and background climate changes. *Climate Dyn.*, **53**, 5999–6033, https://doi.org/10.1007/s00382-019-04913-y.

Ventrice, M. J., and C. D. Thorncroft, 2013: The role of convectively coupled atmospheric Kelvin waves on African easterly wave activity. *Mon. Wea. Rev.*, **141**, 1910–1924, https://doi.org/10.1175/MWR-D-12-00147.1.

——, ——, and M. A. Janiga, 2012a: Atlantic tropical cyclogenesis: A three-way interaction between an African easterly wave, diurnally varying convection, and a convectively coupled atmospheric Kelvin wave. *Mon. Wea. Rev.*, **140**, 1108–1124, https://doi.org/10.1175/MWR-D-11-00122.1.

——, ——, and C. J. Schreck III, 2012b: Impacts of convectively coupled Kelvin waves on environmental conditions for Atlantic tropical cyclogenesis. *Mon. Wea. Rev.*, **140**, 2198–2214, https://doi.org/10.1175/MWR-D-11-00305.1.

Wang, W., 2022: Forecasting convection with a "scale-aware" Tiedtke cumulus parameterization scheme at kilometer scales. *Wea. Forecasting*, **37**, 1491–1507, https://doi.org/10.1175/WAF-D-21-0179.1.

Wheeler, M., and G. N. Kiladis, 1999: Convectively coupled equatorial waves: Analysis of clouds and temperature in the wavenumber–frequency domain. *J. Atmos. Sci.*, **56**, 374–399, https://doi.org/10.1175/1520-0469(1999)056<0374:CCEWAO>2.0.CO;2.

——, and K. M. Weickmann, 2001: Real-time monitoring and prediction of modes of coherent synoptic to intraseasonal tropical variability. *Mon. Wea. Rev.*, **129**, 2677–2694, https://doi.org/10.1175/1520-0493(2001)129<2677:RTMAPO>2.0.CO;2.

Wolding, B., J. Dias, G. Kiladis, E. Maloney, and M. Branson, 2020: Interactions between moisture and tropical convection. Part II: The convective coupling of equatorial waves. *J. Atmos. Sci.*, **77**, 1801–1819, https://doi.org/10.1175/JAS-D-19-0226.1.

Yang, G.-Y., B. Hoskins, and J. Slingo, 2003: Convectively coupled equatorial waves: A new methodology for identifying wave structures in observational data. *J. Atmos. Sci.*, **60**, 1637–1654, https://doi.org/10.1175/1520-0469(2003)060<1637:CCEWAN>2.0.CO;2.

——, ——, and ——, 2007: Convectively coupled equatorial waves. Part I: Horizontal and vertical structures. *J. Atmos. Sci.*, **64**, 3406–3423, https://doi.org/10.1175/JAS4017.1.

Zawislak, J., and E. J. Zipser, 2014: Analysis of the thermodynamic properties of developing and nondeveloping tropical disturbances using a comprehensive dropsonde dataset. *Mon. Wea. Rev.*, **142**, 1250–1264, https://doi.org/10.1175/MWR-D-13-00253.1.

Zhang, G., Z. Wang, T. J. Dunkerton, M. S. Peng, and G. Magnusdottir, 2016: Extratropical impacts on Atlantic tropical cyclone activity. *J. Atmos. Sci.*, **73**, 1401–1418, https://doi.org/10.1175/JAS-D-15-0154.1.